EFDA–JET–PR(08)34

K.D. Lawson, I.H. Coffey, J. Zacks, M.F. Stamp
and JET EFDA contributors

An Absolute Sensitivity Calibration of the JET VUV SPRED Spectrometer

An Absolute Sensitivity Calibration of the JET VUV SPRED Spectrometer

K.D. Lawson[1], I.H. Coffey[2], J. Zacks2, M.F. Stamp[1]
and JET EFDA contributors*

JET-EFDA, Culham Science Centre, OX14 3DB, Abingdon, UK

[1] EURATOM-UKAEA Fusion Association, Culham Science Centre, OX14 3DB, Abingdon, OXON, UK
[2] Astrophysics Research Center, School of Mathematics and Physics, Queen's University, Belfast, BT7 1NN, Northern Ireland, UK
** See annex of F. Romanelli et al, "Overview of JET Results",*
(Proc. 22 [nd] IAEA Fusion Energy Conference, Geneva, Switzerland (2008)).

Preprint of Paper to be submitted for publication in
Journal of Instrumentation

ABSTRACT

The determination of a good relative and absolute sensitivity calibration for wideband VUV spectrometers is challenging. On JET, the possible T and Be contamination of the VUV spectrometer precludes its removal to a synchrotron source and, consequently, a range of alternative *in situ* techniques have been investigated in depth. This has resulted in a reliable calibration for the complete spectral range, the relative calibration at short wavelengths being particularly accurate. At these wavelengths, a novel approach is used, in which the calibration is extended using a number of Na- and Li-like metal doublets. At longer wavelengths, the Lilike doublets of Ar and Ne have been used in conjunction with CII, CIII and CIV line intensity ratios. Unexplained discrepancies between the measured and modelled C results has meant that the exceptional short wavelength accuracy has not be repeated at these longer wavelengths. The absolute sensitivity has been determined from branching ratios to an absolutely calibrated visible spectrometer. The long term stability of the calibration is discussed.

1. INTRODUCTION

Spectral lines from a wide range of elements and ionization stages fall in the VUV spectrum making this a particularly valuable spectral region for diagnosing high temperature plasmas, such as in the JET tokamak. As well as determining elemental impurity concentrations, the VUV spectral line intensities can be used in both core and edge impurity transport analyses. In order to exploit fully the line intensity measurements, an absolute sensitivity calibration for this spectral region is of crucial importance.

The VUV survey spectrometer used on JET is a Princeton Instruments SPRED spectrometer, known as KT2 within the JET team [5]. This routinely observes the spectrum between 100 and 1100Åand is described in section 2. Its wavelength range and routine use makes this instrument ideal for the reference spectrometer for the XUV / VUV suite of spectrometers on JET. The sensitivity depends on a number of factors, the throughput of radiation into the spectrometer, which is defined by the instrument's acceptance angle, the optical behaviour of the slit and grating and the characteristics of the detector.

A comparison of a measured spectral line intensity ratio with the theoretical result from the collisional-radiative population model allows the sensitivity at two wavelengths to be related. The use of further ratios allows the calibration defined in this way to be extended to other wavelengths. To obtain an absolute sensitivity an *in-situ* branching ratio to an absolutely calibrated visible spectrometer is preferred to the use of a standard source. The latter for vacuum instruments is always problematic experimentally and geometrical uncertainties in filling the aperture of the spectrometer by a close source compound these problems.

Section 3 gives the details of the measurements made and of the theoretical models used. The measurements of the branching ratios to an absolutely calibrated visible spectrometer are described in section 3a. In addition to giving an absolute sensitivity, it is also possible to use the branching

ratios to connect the short and long wavelength VUV calibrations. At short wavelengths, a number of Na- and Li-like metal line intensity ratios were used to give the sensitivity and these have resulted in an exceptionally accurate calibration, which extends down to 128Å. The use of these ratios and of two noble gas Lilike ratios to derive the calibration is explained in section 3b.

Ni is routinely observed in the JET plasma, with the Ni lines at 118Å being a useful monitor of this impurity. Since the SPRED sensitivity is expected to fall sharply at wavelengths below ~100Å an extrapolation of the calibration from 128Å to 118Å is thought unreliable. As described in section 3c, the sensitivity at 118Å is obtained by making a cross-calibration to the XUV Schwob-Fraenkel spectrometer, whose sensitivity is more slowly varying in this wavelength range.

At longer wavelengths, >360Å, the Li-like Ar and Ne doublets, together with comparisons of measured and modelled CII, CIII and CIV line intensity ratios are used to give the calibration. The agreement between the experimental and theoretical C data was not found to be as good as for the metal doublets and this is discussed in section 3d. Finally, the long term stability of the sensitivity calibration is described in section 3e. This has implications both for the technique used to obtain the absolute sensitivity calibration and for the construction and calibration of VUV spectrometers on future machines such as ITER.

2. EXPERIMENTAL ARRANGEMENT

The JET VUV survey spectrometer is a Princeton Instruments SPRED instrument [5], which can use one of three toroidal holographic gratings with either 290, 450 or 2105g.mm^{-1} rulings. The 70.6° angle of incidence of the instrument restricts the minimum wavelength to about 100Å and with the 450g.mm^{-1} grating, routinely used on JET, the spectral range extends to 1100Å, with a spectral resolution of ~5Å. The sensitivity calibration has been determined for this grating.

The toroidal holographic grating is designed to give a flat focal field, the central area of the line profiles being the same throughout the spectrum. The only variation that occurs in the profiles are in the line wings, which are found to be somewhat higher at long wavelengths. Normally, the even order spectra are suppressed in the SPRED instruments making the first and third orders the dominant spectra observed. However, the second order spectrum is now seen weakly with the JET instrument. The detector consists of a microchannel plate coated with CuIand a phosphor coupled by a fibre optic bundle to a Reticon photodiode array. After some years of use, the detector was modified so as to double the number of pixels in the photodiode array to 2048. However, it is noted that alternate pixels are amplified independently and some of the data for the present calibration were recorded during a period when one of the amplifier chains had failed (Pulse No's: 55717 to 63445), leaving only 1024 pixels to cover the full wavelength range, this essentially returning the spectrometer to its former setup.

The instrument was initially situated inside the JET torus hall about 5m from and viewing the core plasma along a near horizontal line of sight. To enable measurements to be made during JET T campaigns, the spectrometer was resited outside the torus hall, a distance of 22m from the plasma

[3]. It views the plasma along the vessel midplane via a spherical mirror with an angle of incidence of 15°. The mirror has a Au coating, this arrangement leading to a reduction in the sensitivity of only ~0.5.

In obtaining measurements of the line intensity, use was made of the similarity of the central area of the line profile throughout the SPRED spectrum. A simple and reliable line integration technique was used, in which Simpson's rule is applied to the area defined by a certain number of pixels on either side of the line centre, these pixels also defining the background to be subtracted. With 1024 pixels, an integration range covering ±3 pixels from the line centre was regarded as the best compromise between minimizing blending and using a sufficient proportion of the line profile to ensure reliable measurements. With all 2048 pixels a ±5 pixel range is preferred. This method has been found to be particularly successful when integrating weak lines and when the spectrum is crowded, as is often found at short wavelengths in the SPRED spectrum. Generally, it is much simpler and often more reliable than line fitting. However, there are some cases where line fitting is essential. More details of the line fits required for the CIII and CIV lines used in this analysis are given by [6].

These authors also discuss the measurement accuracy. Although a measurement reproducibility of ~2% was typical for the line intensity ratios being used, with so few pixels in a line profile, ~5 FWHM for 1024 pixels (~10 FWHM with all 2048 pixels), it is also necessary to take account of the position of the pixels within the line profile. This was done by checking the variation in measurements over a period in which there were a number of small pixel shifts; these are due to limitations in the mechanical stability of the instrument. For moderately intense lines, with a peak intensity in the line profile of $\geq 1.7\times10^{5}$cts.s^{-1}, which are well separated from their neighbours, an accuracy of ~6% was achieved for the line intensity ratios.

3. DERIVATION OF THE SENSITIVITY CALIBRATION

A) BRANCHING RATIO CALIBRATIONS WITH THE VISIBLE SPECTRUM

Visible spectrometers can be calibrated using a standard lamp more reliably than is possible for VUV or XUV instruments. The use of a standard source with vacuum instruments is experimentally difficult and the determination of the geometric factor that is usually needed to account for underfilling of the instrument's acceptance angle by the close coupled source introduces uncertainties into the absolute calibration. Indeed, the changes in the long term stability of the absolute sensitivity described in section 3e further add to the uncertainties of any calibration made remote from the machine. Consequently, the absolute sensitivity calibration was found, *in-situ*, by using C branching ratios to crosscalibrate with an absolutely calibrated visible spectrometer with a horizontal line of sight along the same beamline used by the SPRED instrument. C is the dominant low Z element routinely observed in the JET spectrum due to the use of carbon fibre composite, plasma facing components in the machine. The branching ratios used are listed in table 1. On JET, the visible spectrometer with the most reliable absolute calibration has a vertical line of sight and bremsstrahlung continuum

from the plasma was used to crosscalibrate between the vertical and horizontal visible spectrometers. The CIV atomic data was generated specifically for the present analysis by [1] and that for CIII is taken from a review by [2].

The spatial variation in emission from the plasma edge can lead to a wide range of results when comparing intensities of the same spectral line observed with different spectrometers. This is particularly so when using the Xpoint phase of the discharge, for which the variation in the ratio of the line intensities can be up to a factor of ~5. Even when the instruments use the same beamline the range of the ratios can still be ~2. It is therefore essential to use data from a large number of pulses and a range of configurations, the median of the results being preferred. Over a period of time changes in the absolute sensitivity calibration were observed and the long term stability of the sensitivity is discussed in section 3e. Generally the changes were within ±30% of a median value of the absolute inverse sensitivity at 312.4Å of 2.2×10^{12} ph/m^2.sr.cts. Given the ±30% absolute accuracy of the visible line intensities, the absolute accuracy of the VUV calibration is expected to be ±45%.

Use was also made of the proximity of the branching ratio lines in the visible spectrum. The relative sensitivities at 5696Å and 5805Å can be determined with good accuracy, this allowing the sensitivities at the corresponding VUV lines at 574.3Å and 312.4Å to be related. This proved to be particularly valuable given the uncertainties in the C line ratio calibration described in section 3d.

B) NAAND LILIKE DOUBLETS

The Na- and Li-like doublets of a number of intrinsic metallic impurities can dominate the short wavelength VUV spectrum as can be seen in figure 1, which shows intense Cr, Mn, Fe, Ni and Cu lines, recorded between times 6.1 and 7s in pulse 59385. The doublets correspond to the $2p^6 3s\ ^2S1/2 - 2p^6 3p\ ^2P_{1/2,3/2}$ and $1s^2 2s\ ^2S_{1/2} - 1s^2 2p\ 2P_{1/2,3/2}$ transitions, respectively. In addition, elements such as Zr and Mo can be introduced into the plasma by laser ablation and the noble gases Ne, Ar and Kr by gas puffing. The doublets of these elements are ideal for determining the sensitivity calibration of the short wavelength region of the VUV spectrum and in the case of Ne and Ar extending the calibration to higher wavelengths. The line intensity ratios are modelled using the collisionalradiative model, in which the energy level populations are determined from electron collisional excitation and deexcitation and radiative decay. They are found to be insensitive to ne and are only very weakly dependent on T_e.

Ratios were calculated at the temperature corresponding to the ionization potential and at half and double this temperature. Since the ratios differed by less than 2% over this wide temperature range, the values for the central temperatures were adopted. [7, 11] have provided relativistic distorted wave calculations for the electron collisional excitation rates for, respectively, the Naand Lilike ionization stages for a wide range of elements and there are Rmatrix calculations for ArXVI and FeXXIV by [10]. Comparisons of the line intensity ratios modelled using the different electron rates, calculated with the ADAS atomic data package [9], show agreement to within ~1%. Interpolated values were obtained for those elements for which there are no published data and an adjustment

was made to account for the marginally higher (~1%) ArXVI and FeXXIV Rmatrix values. It is expected that the derived line intensity ratios are accurate to a few per cent.

As usual in analysing VUV survey spectra, line blending proved to be a significant problem. Some ratios, such as the CuXIX ratio, were entirely excluded from the analysis; in this case, the longer wavelength line of the doublet at 303.6Å is blended with the 303.8Å HeII line. Despite using only those pulses in which the doublet spectrum of interest was particularly intense, a careful selection of the available data was still necessary in order to give reliable measurements. For example, it was only possible to use 29 of the 51 pulses initially found for the FeXXIV, 192.0Å/255.1Å line ratio due to blending with HeII, CIV, CV, OIV, OV or NiXVII!

A total of 12 Na- and Li-like line intensity ratios were used in deriving the calibration, all but the NeVIII ratio falling in the wavelength range 128Å to 389Å. They are listed in tables 2 and 3, in which their wavelengths, ionization potentials and the modelled line intensity ratios are given. By comparing the measurements with the modelled line intensity ratio, a ratio of the sensitivities at the doublet wavelengths was derived. Most of the wavelength intervals covered by the doublets overlap, there being small gaps from 279.7Å to 292.0Å and from 320.6Å to 335.4Å. This can be seen in figure 2, which shows the wavelength extent and inverse sensitivity ratios of the various doublets. Where the ratios overlap, the sensitivity of the intermediate wavelength is found by interpolating the logarithm of the sensitivity, this allowing the calibration to be extended to lower or higher wavelengths. Small adjustments were made to give the smoothest calibration curve. Crucially, it is noted that two of the most reliable ratios, those for CrXXII and NiXXVI were used to extend the sensitivity from 280Å down to 165Å; hence, there is no concern that successive extensions might progressively increase the error in the calibration curve. To bridge the two gaps in the wavelength coverage, the gradient of the logarithm of the sensitivity curve was taken to be the mean of those on either side. Measurements were made in as many pulses as possible over a range of ~7400 pulses, Pulse No's: 55979 to 63395.

Tables 4 and 5 give comparisons for the Na- and Li-like doublet lines, respectively, of the modelled and measured intensity ratios, together with the derived inverse sensitivity ratios, the number of pulses averaged in obtaining a measurement and estimates of their reliability. During the period in which data were recorded, there were a number of small pixel shifts. As already discussed, there are a limited number of pixels in a line profile and consequently the small pixel shifts led to slightly differing profiles. The more profiles used, the more representative and, therefore, reliable the measurement was considered to be.

As can be seen in figure 3, the relative inverse sensitivity curve (S1 at 312.4Å = 1) derived is close to a straight line in logarithmic space below a wavelength of ~360Å, this being particularly so between 223Å and 360Å. Such behaviour may be understood in that a number of the parameters determining the sensitivity are slowly varying in this wavelength region. It follows that the errors in the extrapolations across the gaps in the wavelength coverage will be minimal and generally gives confidence in the derived calibration in this the most crowded region of the VUV spectrum, where blending can cause severe difficulties in any analysis. Furthermore, if it is supposed that the

calibration should be straight between 153Å and 360Å, then deviations of the derived calibration from this line give some indication of the typical accuracy that might be expected for the relative calibration. For example, the derived calibration at 192Å is only 6% lower than a straight line drawn between the inverse sensitivities at 153Å and 360Å. This figure is the same as would be expected from the measurement accuracy of the line intensity ratios and suggests a very satisfactory accuracy for a calibration in the VUV spectral region. The KrXXVI lines are found to be exceptional in that despite the lines being intense and the time histories wellmatched the derived sensitivity ratio did not fit with the other data. It was not clear from a cross-calibration to the Schwob-Fraenkel spectrometer, which of the KrXXVI lines was in error. The 179.0Å line tended to lie above the general trend of the cross-calibration; the220.0Å line was certainly below. Possible blends, both with first order and higher order lines, have been checked, but with no obvious candidates being found.

Although the measurement of the ArXVI ratio was complicated by blending of the 389.1Å, longer wavelength member of the doublet with the intense CIV line at 384.1Å and is not considered particularly reliable, all the measurements of this ratio do indicate a rise in the inverse sensitivity at this wavelength. Such a sharp rise is most likely due to changes in the quantum efficiency of the CuI coating on the MCP. The intensity of the CIV line at 312.4Å was used to monitor the CIV intensity and, in making a choice of the pulses from which to determine the mean Ar intensity ratio, most weight was given to those pulses for which the ArXVI to CIV, 312.4Å ratio was highest.

The NeVIII doublet has a rather limited wavelength separation of only 10Å. Nevertheless, it was used in conjunction with the C line intensity ratios to derive the calibration at wavelengths longer than 390Å as described in section 3d.

C) SENSITIVITY CALIBRATION AT 118Å

The sensitivity of the SPRED spectrometer falls off sharply at wavelengths less than 100Å due to the grating's non-grazing angle of incidence. The metal Na- and Li-like doublets allow the instrument to be calibrated down to a wavelength of 128Å, but because of the expected fall off in sensitivity it is thought unreliable to extrapolate the calibration below this wavelength. There is a useful Ni line, a NiXXV / NiXXIV / NiXXII blend, at 117.9Å, which is often used to monitor Ni in the JET tokamak and a calibration for this line is desirable.

This has been achieved by a cross-calibration with the Schwob-Fraenkel spectrometer [8], whose wavelength range overlaps that of the SPRED instrument and whose sensitivity is slowly varying in this spectral region. The crosscalibration has been used to determine the sensitivity calibration of the Schwob-Fraenkel spectrometer at wavelengths longer than 128Å, but it also allows the SPRED 118Å sensitivity to be fixed. The details of the crosscalibration are given by [4]. It is confirmed that not only does the SPRED sensitivity fall off even at ~118Å, but also that there is a significant change in the sensitivity at this wavelength over the period for which the calibration has been determined. This is thought due to the ageing of the grating and is illustrated in section 3e, which deals with the longterm stability of the calibration.

D) CII, CIII AND CIV LINE INTENSITY RATIOS

At wavelengths longer than 389Å, only one suitable Na- or Li-like doublet has been found, the NeVIII lines at 770.4Å and 780.3Å. The small wavelength separation makes this doublet of only limited use and additional features of the spectrum must be employed to determine the long wavelength sensitivity calibration. CII, CIII and CIV lines occur throughout this spectral region as can be seen in figure 4, which shows the spectrum for pulse 56016 averaged between times 4 and 10s. Comparisons of measured and modelled line intensity ratios can be used in a similar way to that described in section 3b for the Naand Lilike transitions at shorter wavelengths. In the case of the C ratios, however, there is an additional complication in that the line ratios have some temperature dependence, although at densities $\leq 10^{19} m^{-3}$, typical of the SOL, the CIII and CIV ratios have no significant density dependence. In addition, the sensitivity at 574.3Å can be related to that at 312.4Å through the CIII and CIV branching ratios with the visible spectrum, as has been mentioned in section 3a.

When comparing edge impurity measurements, the most consistent results are obtained with small bore plasmas or during the limiter phase of a discharge. For this analysis, the latter was used for measurements of the C line intensity ratios. This phase also has the advantage that, along a horizontal line of sight, the C intensities tend to be higher than during the X-point phase, C usually dominating the spectrum. This increases the reliability of the measurement, resulting in a more accurate line integral and minimizing line blending. In addition the limiter phase is usually repeated for a number of pulses allowing the reproducibility of the measurements to be checked and the accuracy to be improved further by averaging. Each line intensity ratio used is an average of the measurements from typically 6 pulses. For CII and CIII, a selection of 7 pulse ranges covering the full temperature variation found for CIV was made.

Although there was some agreement between the measured and modelled CIII and CIV data, the agreement was poorer than expected, being significantly worse than the experimental error of ~6%. This contrasts with the Na- and Li-like doublet comparisons, which appear to be limited only by the accuracy of the measurements. For example, three CIII and three CIV lines fall at wavelengths below 389Å, for which the sensitivity calibration has been determined from the Na- and Li-like doublets. In the case of CIV, the T_e of the plasma region emitting radiation from this ion was derived from the 312.4Å/289.2Å line intensity ratio and the sensitivity at 384.1Å and 419.6Å found using the modelled results appropriate to the particular T_e. It is noted that the CIV 384.1Å line is blended with the CIII 386.2Å line and must be treated by fitting Gaussians to the line centres as described by Lawson *et al*. (2009). The resulting 384.1Å inverse sensitivity is ~40% higher than expected. That derived for 419.6Å is found to be different for each of the pulse ranges used, the value depending on the T_e derived from the 312.4Å/289.2Å line ratio, as shown in figure 5.

Two of the three CIII lines found below 389Å are blended at 371Å and consequently their integration requires line fitting [6]. The ratio of the 371Å lines with the 341.2Å line, although not particularly temperature sensitive, also allows a check on the model. The measurements were found

to be 3045% lower than the modelled results, the spread resulting from the estimate of T_e for CIII, although it should be noted that agreement was not possible for any value of T_e. The discrepancies between the C modelled and measured results and an investigation into possible causes are discussed by [6]. As a consequence, the same accuracy as achieved for the short wavelength calibration has not been repeated at longer wavelengths. It is likely that the errors mentioned above, ~30-45%, give an indication as to the accuracy of the sensitivity calibration in this wavelength region, this accuracy being more typical of many VUV calibrations

In the collisionalradiative model, the electron collisional excitation rates depend on T_e and hence this parameter must be known in order to apply the model. Whereas T_e for the CIV emitting plasma region can be obtained from the 312.4Å/289.2Å line ratio, no suitable ratio has been found to give T_e for CIII or CII, and so a choice must be made for these lower ionization stages. The transport of the impurity ions generally leads to them occurring in a plasma region with a higher Te than the temperature of maximum ion abundance under ionization equilibrium (T_{emax}). The other characteristic parameter associated with the temperature of the emitting plasma is the Ionization Potential (IP). A first estimate of the CIII and CII T_e, T_{eC} was made by supposing the same proportion of the IP-T_{emax} interval as for CIV, that is (T_{eC}-T_{emax}) / (IP-T_{emax}) is the same for CII and CIII as for CIV. This leads to a minimum and maximum T_{eCIII} corresponding to the minimum and maximum T_{eCIV}. However, there is evidence from [6] that such a correspondence between the electron temperatures is weak, that is that a high CIV Te does not necessarily lead to a high CIII T_e. Arbitrarily, the CIII T_e was allowed to vary between its minimum and maximum values and for each point in this range the CIV to CIII *gradient* maintained to give the CII T_e. This procedure is illustrated in table 6. Hence, for each pulse range and CIV T_e, there is a range of CIII and CII temperatures for which a range of sensitivity ratios is derived. All points within a range and for all pulse ranges were averaged in deriving the preferred ratio of sensitivities. As with the Na- and Li-like modelling, ADAS was used to calculate the modelled line intensities.

The line intensity ratios used to obtain the long wavelength sensitivity curve are listed in table 7 and figure 6 shows the derived calibration curve relative to S^{-1} at 312.4Å, together with the spread of inverse sensitivities due to variations in T_e for the different pulse ranges used; each pulse range is represented by a different vertical line or in the case of the 419.6Å line the single vertical line indicates the full range of the derived inverse sensitivities, T_e being defined by the 312.4Å/289.2Å ratio. The CIII and CIV branching ratios are of particular value in that they allow the long and short wavelength sections of the calibration curve to be reliably connected, without the uncertainties found when applying the collisionalradiative model to C. A cubic curve was chosen for the fit, initially the coefficients being adjusted so that the curve passed through the inverse sensitivities at 389.1Å and 574.3Å. However, this choice led to there being a significant, ~100%, difference between the fitted curve and the inverse sensitivity at 419.6Å derived from the CIV line intensity ratios. Where comparisons can be made, they suggest typical errors smaller than this and, consequently, a curve passing through a point ~40% of its value lower than the inverse sensitivity at 419.6Å was preferred. The 977.0Å/574.3Å and 904.1Å/594.9Å ratios were used to fix the curve at long wavelengths. Good agreement was found between the

curve derived in this way and the 904.1Å/687.2Å and 780.3Å/770.4Å ratios, despite concerns of possible blending of the 687.2Å line with the CIII line at 690.5Å. The least satisfactory ratio, for which agreement with the preferred curve was poorest, was the 538.2Å/459.6Å line ratio. For this ratio, the spread in sensitivities due to variations in T_e is relatively small and so its poor agreement cannot be explained by the choice of CIII temperatures. It is noted that in figure 6 the 904.1Å data that forms part of the 904.1Å/687.2Å ratio has been shifted by 8Å to avoid confusion.

Given the arbitrary way in which the temperature ranges for CIII and CII were chosen, a further check was made on the sensitivity of the derived calibration curve to the choice of T_e. Increasing T_e by 1 and 2eV for CII and CIII, respectively, still gave results within the expected errors of ~45%. However, reducing the temperatures by a similar amount, which increases the temperature dependence of all the ratios considered, led to significantly larger displacements of the optimized curve at the longest wavelengths, +84% and +110% at 904.1Å and 977.0Å, respectively. It was necessary to limit the reduction in the CII and CIII temperatures to ~0.5 and 1eV, respectively, to stay within the ~45% accuracy at all wavelengths. The resulting curves are shown in figure 7. It can be seen that, throughout most of the wavelength range (λ800Å), uncertainties due to the application of the collisionalradiative model dominate any due to the choice of temperature.

E) LONG TERM STABILITY OF THE SENSITIVITY CALIBRATION

For diagnostics used routinely on machines such as JET, which have long periods of operations with little intervention possible, it is not only necessary to define the sensitivity calibration at one particular time, but also to monitor the stability of the sensitivity throughout the periods of operations. To illustrate the importance of such a procedure, three examples are given of changes in the sensitivity of the JET SPRED spectrometer.

The first relates to changes in the relative sensitivity between different wavelengths within the spectrum. Such changes are normally seen as small drifts. However, more significant jumps in the sensitivity are occasionally observed. This was the case after the shutdown at the end of the 1999 operations, the sensitivity change being accompanied be a pixel shift of ~10 pixels. It is found that the intensities of certain C lines recorded early in the limiter phase of a discharge are reproducible from pulse to pulse and this is used to monitor the stability of the sensitivity, together with comparisons of measurements of the same C lines made by other spectrometers. Figure 8 shows the mean of the intensities at times 3.5 and 4.0s of the CIV line at 312.4Å and the CIII lines at 574.3Å and 977.0Å averaged over ~30 to 50 pulses plotted against JET pulse number. At 312.4Å there is a drop in the sensitivity between Pulse No's: 49795 and 49931 approaching ~20%, which recovers, whereas at 574.3Å and 977.0Å there is a jump of ~30%, which does not recover. The change in the relative sensitivity between 312.4Å and 574.3Å is confirmed by measurements of the branching ratios to the visible spectrum; these suggest that at this time there was a change of ~24% in the sensitivity between these wavelengths.

In another example, the step in the sensitivity more clearly affects the whole spectrum. Such

steps are often combined with a smaller change in the relative calibration. In figure 8, a clear increase in the sensitivity is seen at all wavelengths after pulse 52210, this being the last pulse before a weekend break in operations. This jump in sensitivity is confirmed by crosscalibrations with the Schwob-Fraenkel and visible spectrometers. At 312.4Å the jump is ~35%, at 574.3Å ~40% and at 977.0Å approaching 70%. The precise reasons for the changes in the relative and absolute sensitivities described above are not understood. Neither are thought due directly to operations, since the instrument is situated at the end of a long beamline. Changes in the relative calibration must be internal to the spectrometer, this emphasizing the need for a very stable mechanical design.

Finally, the change in the sensitivity at 118Å has been monitored. Over the many years of operation a significant fall in the sensitivity at 118Å has been observed. This is illustrated in figure 9 and is thought due to the ageing of the grating. It is also noted that the holographic grating used should suppress the even orders of the spectrum; however, after years of operation the second order has been observed and is slowly becoming more intense. Figure 9 was derived through a crosscalibration with the SchwobFraenkel XUV spectrometer, the 118Å sensitivity being related to that at 312.4Å. As discussed above there is a change in the sensitivity between Pulse No's: 49795 and 49931 that is not uniform across the whole spectrum. Additional points have therefore been included in figure 9, which better reflect the falloff in sensitivity at 118Å.

These examples show the importance of monitoring the sensitivity at more than one wavelength in spectrometers used for routine spectral surveys of large machines such as JET and ITER. Clearly, any changes will be minimized by taking great care to ensure mechanical stability when designing new instruments and their ancillary equipment.

The preferred complete inverse sensitivity calibration curve on an absolute scale is shown in figure 10. The relative calibration at short wavelengths was derived using Pulse No's: within the range 55979 to 63395, although, apart from the 118Å point, data for the curve at the very shortest wavelengths, <150Å, was only available for a few pulses in the range 55979 to 57241. The longer wavelength relative calibration used pulses in the range 56016 to 63445. It is noted that, within these ranges, no significant drift or changes in the *relative* calibration were found apart from at 118Å, the change in the inverse sensitivity at 118Å being illustrated for the Pulse No's: 48802 to 63445. The error bars shown in the diagram refer to the relative calibration. The absolute level of the calibration applies to the Pulse No's: 56902 to 59441.

CONCLUSION

A sensitivity calibration for the JET VUV SPRED survey spectrometer has been presented. The relative calibration at short wavelengths has been derived by comparing measured and modelled Na- and Li-like metal line intensity ratios. This gives a particularly accurate calibration, which is expected to be better than ~10% throughout most of this wavelength region (128Å-360Å). Its detail and accuracy is expected to enhance the use of the SPRED spectrometer. A cross calibration to the

JET XUV Schwob-Fraenkel spectrometer allowed the short wavelength calibration to be extended to include the Ni blend at 118Å, at which wavelength the sensitivity was found to fall over the years of the spectrometer's operation. At longer wavelengths, CII to CIV line intensity ratios have been used. Due to discrepancies between the measured and modelled C line intensity ratios that, as yet, are not understood, the accuracy of the short wavelength calibration could not be repeated. The expected accuracy of ~45% is more typical of other VUV calibrations. The absolute calibration has been obtained by an *in situ* cross calibration via branching ratios to an absolutely calibrated visible spectrometer.

Since the survey spectrometer is routinely used to give impurity data for the operation of the JET machine, its longterm stability is of importance and has been assessed. This highlights the need for *in situ* absolute calibrations and for both highly stable mechanical designs and regular checks on the sensitivity during the routine use of these instruments.

ACKNOWLEDEGEMENTS

This work was carried out within the framework of the European Fusion Development Agreement and was partly funded by the United Kingdom Engineering and Physical Sciences Research Council and by the European Communities under the contract of Association between EURATOM and UKAEA. The views and opinions expressed herein do not necessarily reflect those of the European Commission.

REFERENCES

[1]. Aggarwal K.M. and Keenan F.P, 2004, Phys. Scr., **69**, 385

[2]. Allard N., Artru M.C., Lanz T. and Le Dourneuf M, 1990, Astron. Astrophys. Suppl. Ser., **84**, 563

[3]. Coffey I.H., Barnsley R *et al*., 2004, Rev. Sci. Instrum., **75**, 3737

[4]. Coffey I.H. *et al*., 2009, 'An absolute calibration of the JET XUV Schwob-Fraenkel duo-multichannel spectrometer – I', To be submitted to J. Instrum.

[5]. Fonck R.J, Ramsey A.T, Yelle R.V, 1982, Appl.Opt., **21**, 2115

[6]. Lawson K.D. *et al*., 2009, 'Comparison of modelled C VUV line intensity ratios with observations of the emission from the JET plasma SOL– I', JET Report

[7]. Sampson D.H, Zhang H.L, Fontes C J, 1990, ADNDT, **44**, 209

[8]. Schwob J.L, Wouters A.W, Suckewer S, Finkenthal M, 1987, Rev. Sci. Instrum., **58**, 1601

[9]. Summers H.P, 2004, 'The ADAS User Manual, version 2.6 http://adas.phys.strath.ac.uk'

[10]. Whiteford A.D, Badnell N.R, Balance C.P, Loch S.D, O'Mullane M.G, Summers H P, 2002, J. Phys. B, **35**, 3729

[11]. Zhang H.L., Sampson D.H., Fontes C.J., 1990, ADNDT, **44**, 31

Ion	Wavelength (Å)	Transition	A-value
C III	574.28	$2s2p\ ^1P_1 - 2s3d\ ^1D_2$	6.80×10^9
C III	5696.0	$2s3p\ ^1P_1 - 2s3d\ ^1D_2$	4.28×10^7
C IV	312.42	$2s\ ^2S_{1/2} - 3p\ ^2P_{3/2}$	4.51×10^9
C IV	312.45	$2s\ ^2S_{1/2} - 3p\ ^2P_{1/2}$	4.52×10^9
C IV	5801.51	$3s\ ^2S_{1/2} - 3p\ ^2P_{3/2}$	3.28×10^7
C IV	5812.14	$3s\ ^2S_{1/2} - 3p\ ^2P_{1/2}$	3.26×10^7

The visible wavelengths are in air.

Table 1: C III and C IV branching ratio transitions and their Avalues.

Ion	Wavelengths (Å)	Ionization potential (eV)	Modelled intensity ratio	Source
FeXVI	335.4 / 360.8	489	1.95	Intrinsic
NiXVIII	292.0 / 320.6	607	1.94	Intrinsic
KrXXVI	179.0 / 220.0	1205	1.88	Gas puffed
ZrXXX	142.9 / 189.6	1575	1.84	Laser ablation
MoXXXII	127.9 / 176.6	1776	1.82	Laser ablation

Table 2: Nalike doublet modelled line intensity ratios

Ion	Wavelengths (Å)	Ionization potential (eV)	Modelled intensity ratio	Source
NeVIII	770.4 / 780.3	239	2.02	Gas puffed
ArXVI	353.9 / 389.1	918	1.97	Gas puffed
CrXXII	223.0 / 279.7	1722	1.93	Intrinsic
MnXXIII	206.9 / 266.9	1880	1.92	Intrinsic
FeXXIV	192.0 / 255.1	2046	1.91	Intrinsic
NiXXVI	165.4 / 234.1	2399	1.88	Intrinsic
CuXXVII	153.5 / 224.7	2585	1.87	Intrinsic

Table 3: Lilike doublet modelled line intensity ratios

Ion	Modelled intensity ratio	Measured intensity ratio	Inverse sensitivity ratio	Number of pulses	Number of line profiles	Reliability
FeXVI	1.95	1.99 ±2.1%	0.978	26	3	D
NiXVIII	1.94	1.96 ±4.1%	0.989	24	4	B
KrXXVI	1.88	2.79 ±1.9%	0.674	10	1	F
ZrXXX	1.84	1.91 ±3.0%	0.965	16	2	E
MoXXXII	1.82	1.78 ±2.2%	1.021	7	1	F

A indicates most reliable, F least reliable

Table 4: Comparison of Nalike doublet line intensity ratios

Ion	Modelled intensity ratio	Measured intensity ratio	Inverse sensitivity ratio	Number of pulses	Number of line profiles	Reliability
NeVIII	2.02	2.18 ±4.6%	0.928	24	5	B
ArXVI	1.97	2.68 ±8.1%	0.736	13	2	E
CrXXII	1.93	2.04 ±1.7%	0.946	42	6	A
MnXXIII	1.92	2.12 ±2.9%	0.907	6	3	E
FeXXIV	1.91	2.17 ±2.3%	0.881	29	5	C
NiXXVI	1.88	2.00 ±5.7%	0.942	54	7	A
CuXXVII	1.87	1.99 ±3.2%	0.940	11	3	D

A indicates most reliable, F least reliable

Table 5: Comparison of Lilike doublet line intensity ratios

Ion	T_e of max. ion abundance (T_{emax}) (eV)	Ionization potential (IP) (eV)	IP – T_{emax} difference (eV)	T_e range (eV)	Example of choice of T_e ranges (eV)
CIV	7.5	64.5	57.0	11.3 – 15.1 (0.0667) – (0.133)	12.0 (0.0789)
CIII	4.0	47.9	43.9	6.93 – 9.84 (0.0667) – (0.133)	6.93 – 9.84 (0.0667) – (0.133)
CII	1.65	24.4	22.7		2.89 – 5.90 (0.0545) – (0.187)

Example of choice of CIII and CII T_e ranges calculated for a measured CIV T_e of 12eV.
Figures in brackets correspond to the ratio (T_e of C ion – T_{emax})/(IP – T_{emax})
IP is the ionization potential and T_{emax} the temperature of maximum ion abundance under ionization equilibrium.

Table 6: Temperature ranges for CII – CIV.

Ion	Wavelengths (Å)	Transition	Averaged modelled intensity ratio	Averaged measured intensity ratio	Inverse sensitivity ratio
CIV	384.1 / 312.4	$2p\ ^2P_{1/2,3/2} - 3d\ ^2D_{3/2,5/2}$ $2s\ ^2S_{1/2} - 3p\ ^2P_{1/2,3/2}$	1.95	1.026	1.90
CIV	419.6 / 312.4	$2p\ ^2P_{1/2,3/2} - 3s\ ^2S_{1/2}$ $2s\ ^2S_{1/2} - 3p\ ^2P_{1/2,3/2}$	1.69	0.519	3.25
CIII / CIV	574.3 / 312.4	$2s2p\ ^1P_1 - 2s3d\ ^1D_2$ $2s\ ^2S_{1/2} - 3p\ ^2P_{1/2,3/2}$	1.151	0.296	3.89
CIII	538.2 / 459.6	$2s2p\ ^3P_{0,1,2} - 2s3s\ ^3S_1$ $2s2p\ ^3P_{0,1,2} - 2s3d\ ^3D_{1,2,3}$	0.972	0.347	2.80
CIII	977.0 / 574.3	$2s^2\ ^1S_0 - 2s2p\ ^1P_1$ $2s2p\ ^1P_1 - 2s3d\ ^1D_2$	214.8	4.18	51.4
CII	904.1 / 594.9	$2s^22p\ ^2P_{1/2,3/2} - 2s2p^2\ ^2P_{1/2,3/2}$ $2s^22p\ ^2P_{1/2,3/2} - 2s^24d\ ^2D_{3/2,5/2}$	36.4	3.21	11.34
CII	904.1 / 687.2	$2s^22p\ ^2P_{1/2,3/2} - 2s2p^2\ ^2P_{1/2,3/2}$ $2s^22p\ ^2P_{1/2,3/2} - 2s^23d\ ^2D_{3/2,5/2}$	9.46	1.385	6.83
NeVIII	780.3 / 770.4	$2s\ ^2S_{1/2} - 2p\ ^2P_{1/2}$ $2s\ ^2S_{1/2} - 2p\ ^2P_{3/2}$	0.495	0.460	1.077

Table 7: Line intensity ratios used to derive the long wavelength sensitivity calibration.

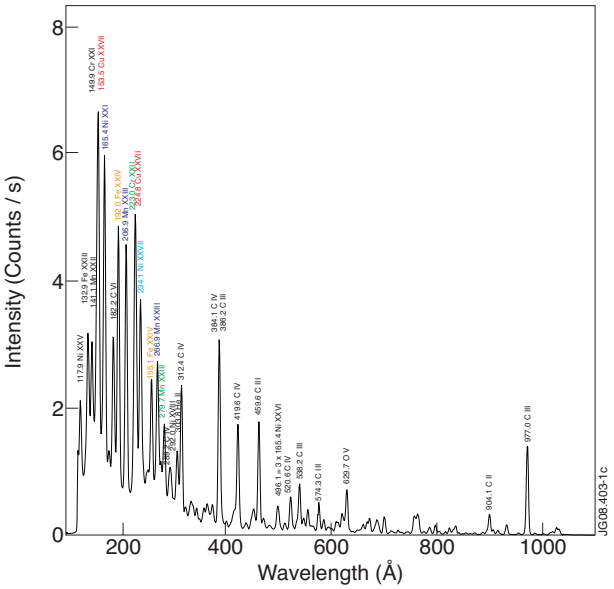

Figure 1: The SPRED spectrum for JET Pulse No: 59385 averaged between times 6.1 and 7.0s.

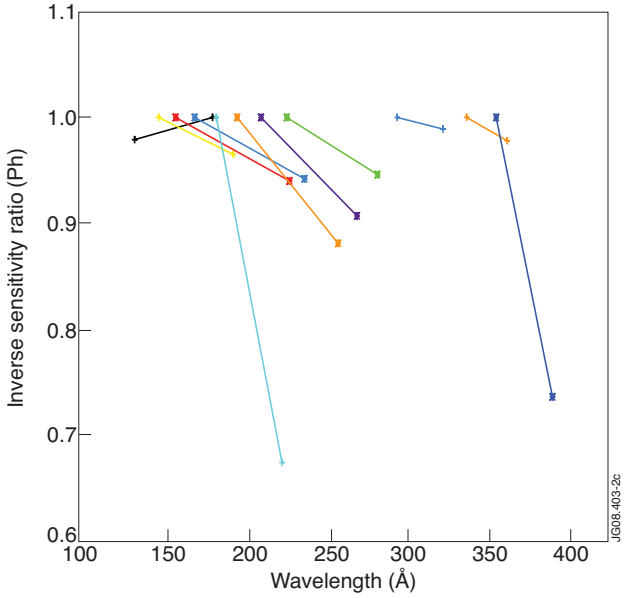

Figure 2: The Na(+) and Lilike (*) inverse sensitivity ratios plotted against wavelength for – Ar, – Cr, – Mn, – Fe, – Ni, – Cu, – Kr, Zr and – Mo.

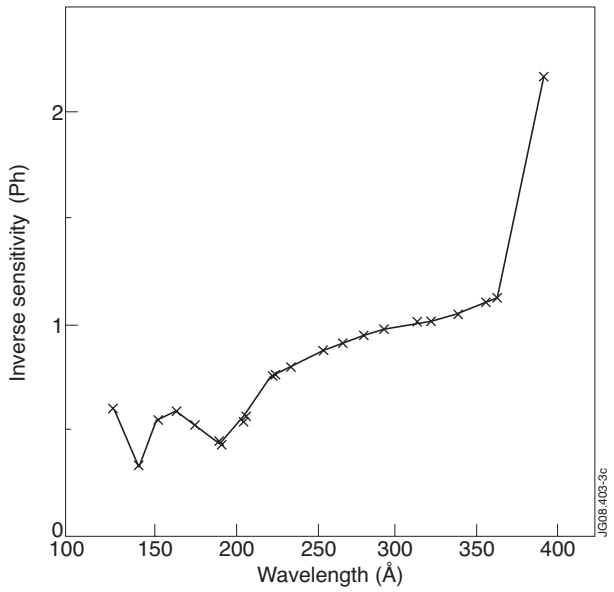

Figure 3: The relative inverse sensitivity calibration at short wavelengths derived from Naand Lilike doublet ratios (S^{-1} at 312.4Å = 1).

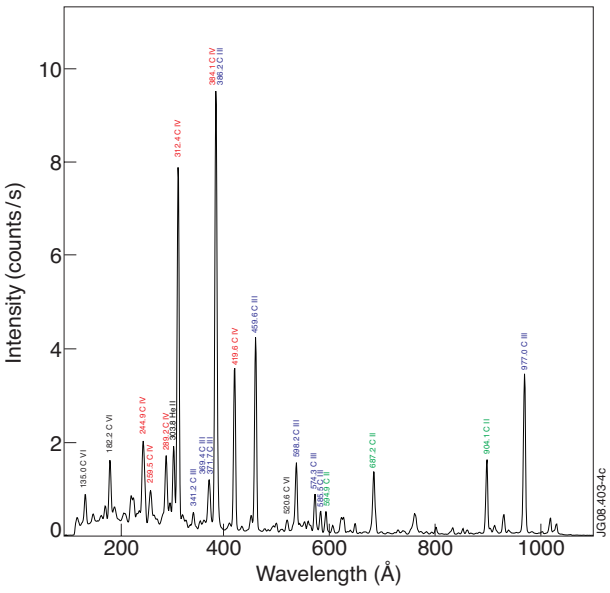

Figure 4: The SPRED spectrum for JET pulse 56016 averaged between times 4 and 10s.

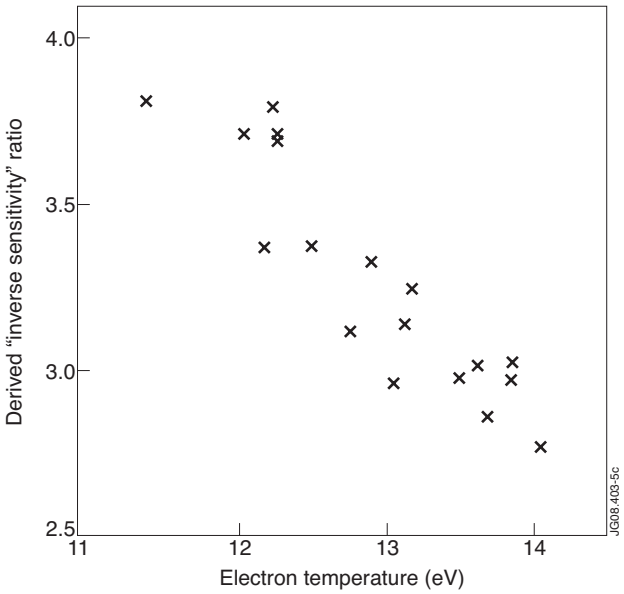

Figure 5: Ratio of the derived 'inverse sensitivity' at 419.6Å to that at 312.4Å plotted against the electron temperature as measured by the 312.4Å/289.2Å line intensity ratio.

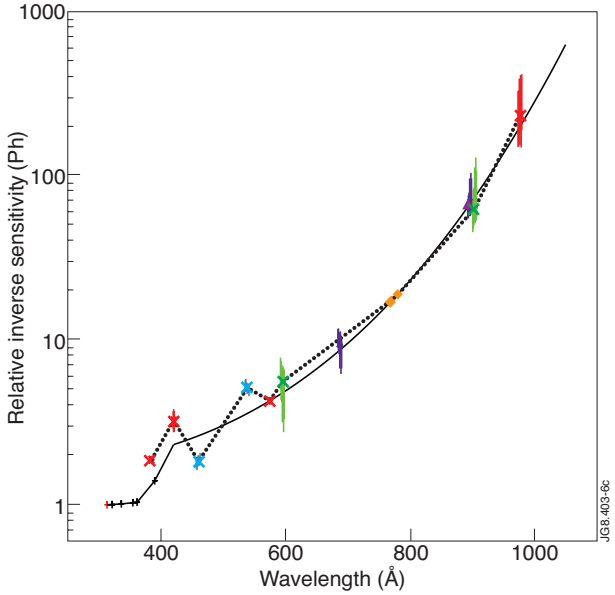

*Figure 6: Relative inverse sensitivity calibration at long wavelengths, derived from C line intensity ratios (S^{-1} at 312.4Å = 1). * S^{-1} derived from CIII and CIV ratios with the 574.3Å and 312.4Å lines. * S^{-1} from CIII 538.2Å/459.6Å ratio. * S^{-1} from CII 904.1Å/594.9Å ratio. Δ S1 from CII 904.1Å/687.2Å ratio used as check. ◇ S^{-1} from NeVIII 780.3Å/770.4Å ratio used as check. + S^{-1} derived from short wavelength Naand Lilike doublet intensity ratios. Vertical lines indicate spread in data for different temperatures and pulse ranges.*

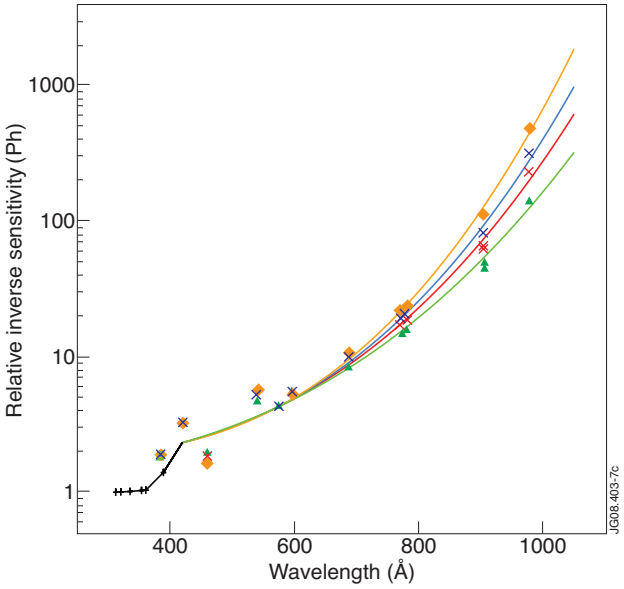

*Figure 7: Relative inverse sensitivity calibration at long wavelengths showing the sensitivity of the calibration to temperature (S^{-1} at 312.4Å = 1). + preferred calibration, * CII and CIII T_e reduced by 0.5 and 1eV, respectively, ◇ CII and CIII T_e reduced by 1 and 2eV, respectively, Δ CII and CIII Te increased by 1 and 2eV, respectively. + S^{-1} derived from short wavelength Naand Lilike doublet intensity ratios.*

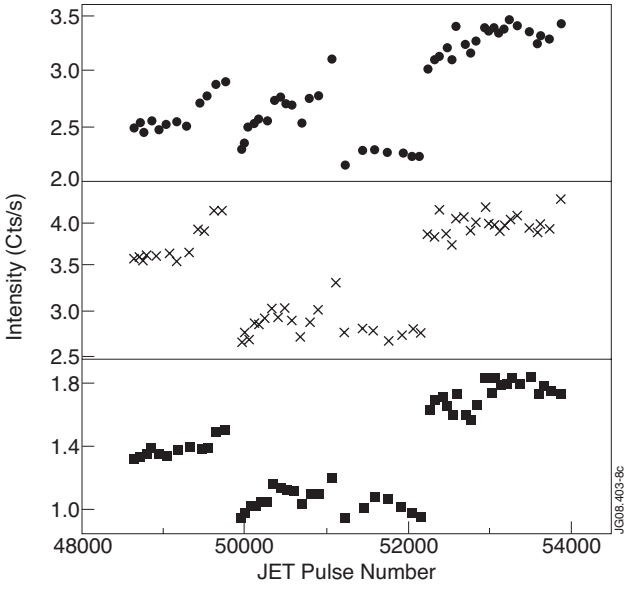

*Figure 8: Mean of the measurements at 3.5s and 4s averaged over ~3050 Pulses for the + 312.4Å, C IV, + 574.3Å, C III and + 977.0Å, C III line intensities plotted against pulse number. + S relative to 312.4Å. * S adjusted to illustrate better its falloff at 118Å.*

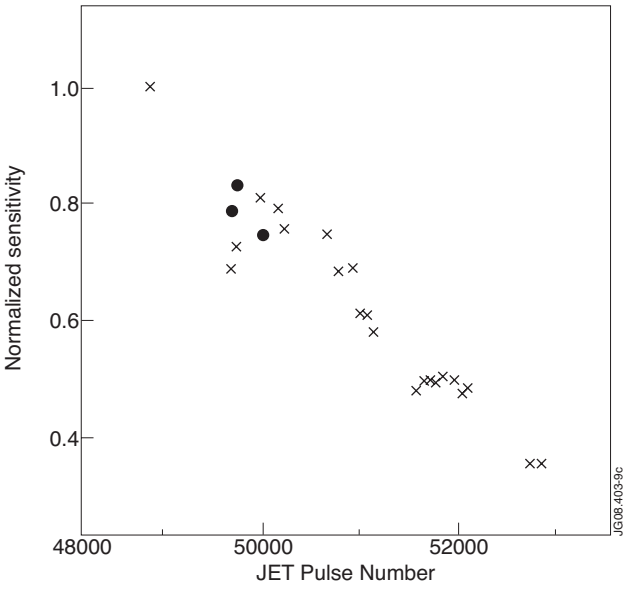

*Figure 9: Variation in the sensitivity at 118Å with pulse number. + S relative to 312.4Å. * S adjusted to illustrate better its falloff at 118Å.*

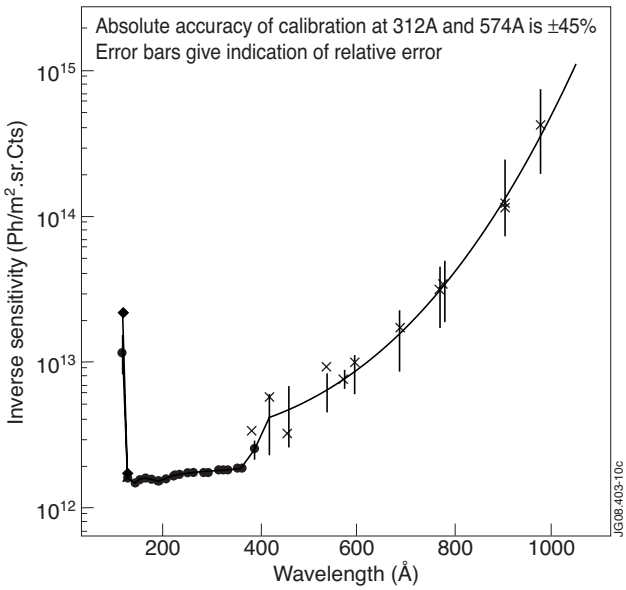

*Figure 10: Absolute inverse sensitivity calibration for the KT2 spectrometer appropriate to Pulse No's: 56902 to 59441. * S^{-1} derived from C and Ne VIII line ratios, x S1 from other Naand Lilike ratios, ◇ S^{-1} at 118Å showing the range of the calibration between Pulse No's: 48802 and 63445.*